Flow of microgel capsules through topographically patterned microchannels

Lindsey K. Fiddes,[a] Edmond W. K. Young,[bc] Eugenia Kumacheva*[a] and Aaron R. Wheeler*[ac]

Received 5th March 2007, Accepted 16th May 2007
First published as an Advance Article on the web 1st June 2007
DOI: 10.1039/b703297h

We investigated the flow dynamics of microgel capsules in topographically patterned microfluidic devices. For microgels flowing through channel constrictions, or orifices, we observed three phenomena: (i) the effect of confinement, (ii) the role of interactions between the microgels and the channel surface, and (iii) the effect of the velocities of microgels prior to their passage through an orifice. We studied negatively charged alginate microgels and positively charged alginate microgels coated with *N*-(2-hydroxy)propyl-3-trimethylammonium chitosan chloride (HTCC). Aqueous dispersions of microgels were driven through poly(dimethyl siloxane) microchannels carrying a weak negative surface charge. The velocity of the continuous phase, and hence, the velocity of the microgels increased as they passed through topographically patterned orifices. Alginate microgels were observed to have a larger increase in velocity relative to HTCC-coated alginate microgels. This effect, which was attributed to electrostatic attraction or repulsion, was found to be strongest for orifices with dimensions close to the microgel diameter. For example, when 75 μm-diameter microgels flowed through a 76 μm orifice, alginate gels (negatively charged) experienced a 2× greater increase in velocity than HTCC-coated (postitively charged) microgels. This effect was exaggerated at lower initial flow rates. For example, when 75 μm-diameter microgels flowed through an 80 μm orifice, a two-fold difference in the velocity changes of the two microgel types was observed when the initial flow rate was 275 μm s^{-1}, while a three-fold difference in velocity changes was observed when the initial flow rate was 130 μm s^{-1}. We speculate that these studies will be useful for modeling the flow of suspensions of cells or other biologically relevant particles for a wide range of applications.

Introduction

Microbeads formed from biopolymer gels, or *microgels*, have a broad range of applications[1,2] in the pharmaceutical,[3,4] nutrition,[5–7] and cosmetic industries,[8,9] due to their stimulus-responsive nature, the ease with which their surfaces can be functionalized, and their capacity to encapsulate and release functional species. For example, microgels are uniquely suited for drug delivery, as they can be loaded with therapeutic and/or diagnostic agents and can transport the agents through biochemical hazards to release them in specifically targeted tissues. In drug delivery and many other applications, the flow characteristics of microgels in constrained geometries are critical to their efficacy. Understanding the behavior of microgels in confined geometries is useful in efforts to formulate and encapsulate new drugs, to tune the kinetics of loading and unloading events, and to increase the levels of penetration to protected tissues in living systems.

Microfluidics has emerged as a powerful tool for evaluating the flow behavior of particles in systems with low Reynolds number. Studies of flow of dispersions of rigid polymer beads,[10–21] micelles,[22] vesicles,[23,24] microgels[5,25–27] and coacervates of oppositely charged constituents[28,29] have been conducted in microfluidic channels. For example, a study of the flow of particles in microchannels of different shapes has been conducted for polystyrene beads.[14] It was found that the particle velocity was reduced when the microbead diameter was comparable to the channel width and when the particle streamline was close to the channel walls. It was also reported that particles entering a gradual contraction (through an angled channel) experienced higher velocities than those entering an abrupt contraction.[14] A study of flow in channels with alternating converging and diverging regions showed that the variation in particle velocity was largest when the particle moved in the centerline of the channel.[15] In addition, many studies have used micro particle image velocimetry (μPIV) to model the behavior of particles in biological environments.[12,30]

Several of the studies described above were applied to model the flow behavior of cells; however, rigid microbeads bear little in common with the heterogeneous structure and mechanical properties of cells. Theoretical studies suggest that a better model of cell transport is the flow of capsules with soft elastic shells.[31,32] We speculate that using compliant microgel capsules[33–35] will be a more accurate model for the flow of cells in constrained geometries. The microgels used here had an average diameter of 75 μm, making them a good model for many eukaryotic cells (which typicallay range from 10–100 μm

[a]*Department of Chemistry, University of Toronto, 80 St. George Street, Toronto, Ontario, Canada M5S 3H6.*
E-mail: ekumache@chem.utoronto.ca; awheeler@chem.utoronto.ca;
Fax: (EK) +1 416 978 3576; Fax: (ARW) +1 416 946 3865;
Tel: (EK) +1 416 978 3576 Tel: (ARW) +1 416 946 3864
[b]*Department of Mechanical and Industrial Engineering, University of Toronto, 5 King's College Road, Toronto, Ontario, Canada M5S 3G8*
[c]*Institute of Biomaterials and Biomedical Engineering, University of Toronto, 164 College Street, Toronto, Ontario, Canada M5S 3G9*

in diameter); however, we note that this size is $\sim 5\times$ larger than common types of mammalian cells.

One important property of particle flow in constrained geometries is the nature of the interactions of particles with channel walls. To our knowledge, only a few studies have attempted to examine the change in particle flow due to attractive forces between the particle and channel surface. For example, Wong *et al.*[36] used a suspension of beads in a flow cell to show that particles modified with streptavidin could interact with biotin patterned on the surface of the cell.

Here we report the results of an experimental study of the flow of capsular biopolymer microgels in topographically patterned microchannels. We describe three features of flow of microgels: (i) the effect of confinement, (ii) the role of surface charge of microgels, and (iii) the effect of the velocities of microgels prior to passage through abrupt contractions in channel width.

Experimental methods

Preparation of microgels

Capsular alginate microgels were prepared using the two-phase microfluidic flow-focusing approach of Zhang *et al.*[35] Briefly, an aqueous solution of sodium alginate was emulsified in a microfluidic flow-focusing device. As the stream of droplets traveled through the downstream channel, calcium crosslinker diffused from the continuous phase (1-undecanol) into the droplets, transforming them into capsules (*i.e.*, liquid cores engulfed by gel shells). In the present work, the concentration of sodium alginate in the aqueous phase was 3 wt%, the concentration of CaI_2 in 1-undecanol was 0.25 wt%, and the time of gelation was 90 s. After exiting the microfluidic device the capsules were transferred to phosphate buffered saline (PBS) solution (pH 7.4). The size of capsules was measured and analyzed using a light microscope (Olympus BX51) and Image Pro Plus Software (Media Cybernetics, Silver Spring, MD). An analysis of 50 particles yielded a mean diameter of microgels of 75 ± 3 μm. An image of the microgels is depicted in Fig. 1A.

In the present work, we used two types of microgels: untreated alginate microgels carrying a negative charge, and alginate microgels coated with *N*-(2-hydroxy)propyl-3-trimethylammonium chitosan chloride (HTCC), carrying a positive charge. The latter were prepared by suspending alginate microgels (0.15 wt% in PBS) in an aqueous 0.16 wt% HTCC solution for 24 h, centrifuging the suspension and re-suspending the particles in PBS.[37] No noticeable change in the size of microgels was observed after the coating procedure.

The value of the ζ-potential of the microgels used in the present work was measured by filling a 40 mm-long glass capillary (id = 1.1 mm) with a dilute dispersion of microgel particles, and applying a potential in the range of 100 to 250 V across the length of the capillary. The capillary was first coated with 3-aminopropyltriethoxysilane (99%, Aldrich) to prevent microgels from adhering to the glass surface. Electroosmotic flow was determined using 2.2 μm-diameter functionalized polystyrene (PS) beads with a ζ-potential of −38 mV. The value of the ζ-potential of microgels was then calculated using the equation[38]

$$v = (U_e + U_o)E$$

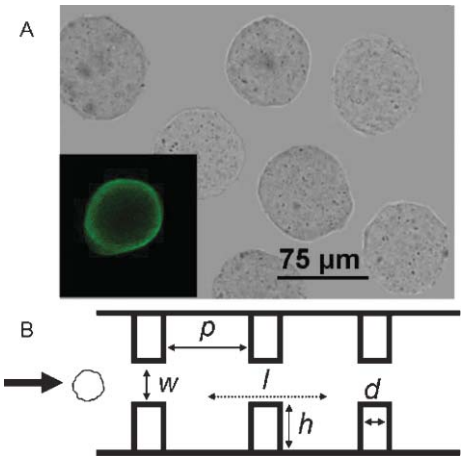

Fig. 1 (A) Optical microscopy image of alginate capsules in PBS solution. Confocal fluorescence microscopy image of alginate capsule labelled with Ca^{2+} indicator, Fluo-3 (inset, adapted with permission from Zhang *et al.*[35]). (B) Schematic of the ten-orifice microchannel, with dimensions: d = 100 μm, h = 500 μm, and p = 2 mm. The depth of the channel is 150 μm. The width, w, of the orifice varied from 76 μm to 200 μm. The mean microgel diameter is 75 μm. The path, l, over which microgel velocity was measured, is 1 mm.

where v is the microgel velocity; E is the electric field strength; U_o is the electroosmotic mobility; and U_e is the electrophoretic mobility defined as

$$U_e = 2\varepsilon\zeta f(\kappa a)/3\eta$$

where ε is the dielectric constant of the solvent, $f(\kappa a)$ is Henry's function, κ is the Debye–Hückel parameter, a is the particle radius, and η is the viscosity of the solvent. For ε = 80.1, $f(\kappa a)$ = 1.5, and $\eta = 8.9 \times 10^{-4}$ Pa s, the values of the ζ-potential of alginate particles and HTCC-coated alginate particles were found to be −33 mV and +15 mV, respectively.

Preparation of microfluidic devices

Microfluidic devices were fabricated using the Sylgard 184 Silicone Elastomer Kit (PDMS) (Dow Corning Corp., Midland, MI) by the soft lithography method.[39] Briefly, negative-relief masters were formed from 150 μm-thick SU-8 50 photoresist (MicroChem, USA) on silicon wafers. PDMS pre-polymer was poured onto masters, cured, peeled, and trimmed, and then affixed to glass slides by oxygen plasma bonding. Fig. 1B shows a schematic of the 1.2 mm-wide microchannel containing a series of 10 equally spaced orifices with lengths of 80 μm and mean widths ranging from 76 to 200 μm. The variation in orifice width was found to be $\pm$ 2.9 μm.

Experimental design

We examined the characteristics of flow of negatively charged alginate microgels, positively charged HTCC-alginate microgels and 9.9 μm-diameter PS beads, all dispersed in PBS. The dispersions were sufficiently dilute to avoid particle–particle interactions. To achieve uniform flow of microgel capsules, the dispersions were injected through the microchannel by means of gravity-driven flow. The free end of the inlet tube was

affixed to a reservoir mounted on a translation stage. By controlling the vertical position of the stage with respect to the microfluidic device, we achieved fluid velocities in the microchannel in the range of 0 to 800 μm s^{-1}. Velocities were calibrated by analyzing video frames of PS beads traveling a known distance.

The motion of microgels through orifices was observed under 100× magnification and recorded using a CCD camera. The field of view around the orifice was divided into 22.5 μm-wide segments. The stream-wise velocity of each particle was determined as it passed through each segment. For each experimental condition, we analyzed the flow pattern of 30 microgel capsules to determine the normalized particle velocities $v_n = v/v_w$, where v_n is the normalized velocity, v is the velocity of the observed microgel in the orifice, and v_w is the velocity of the observed gel in the widest part of the channel. As microgels did not always flow in the center of the microchannels, care was taken to calculate velocities only for the microgels that followed the center streamline of the flow. The typical velocity for v_w was 250 μm s^{-1} unless otherwise specified.

Results and discussion

Velocity profile of the continuous phase

While analytical solutions of the velocity profile of fluid moving in channels have been derived[40] we used an approximation proposed by Purday[41] to estimate the values of v and v_w. For fluid in a 1.2 mm wide channel at 10 μm s^{-1}, with orifice width w = 80 μm, a simple conservation of mass calculation shows that the mean and maximum velocities in the orifice are 150 μm s^{-1} and 290 μm s^{-1}, respectively. These results were confirmed numerically by simulating this flow condition using the Fluent computational software package (ANSYS, Inc, Lebanon, NH), as shown in Fig. 2A.

The variation of velocity along the microchannel center axis was also examined experimentally. Normalized plots of velocity as a function of axial distance along channel (where $x = 0$ is defined as the center of the orifice) were generated, and showed good agreement with simulated results. The spatial position of experimentally determined peak velocities were found to consistently coincide with the middle of the orifice at $x = 0$, as shown in Fig. 2B.

Flow characteristics of microgels

The flow characteristics of the negatively charged alginate microgels and positively charged HTCC-coated microgels were evaluated in two series of experiments. First, we studied the effect of varying orifice width on the linear velocity of microgels in the microchannels. Second, we examined the effect of flow rate of the dispersion in the microchannel on the variation in linear velocity of microgels in the orifices. Both types of microgels had a density close to that of PBS solution, and diameters significantly smaller than the depth of the microchannel (150 μm). Thus, it was reasonable to assume that these neutrally-buoyant particles were suspended in the fluid far from the bottom and top surfaces of the channel.

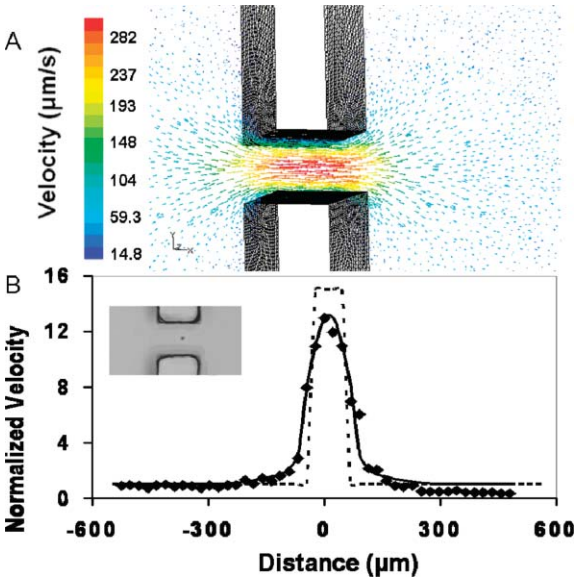

Fig. 2 (A) Simulation of Newtonian fluid flow through an orifice with w = 80 μm. The x-, y-, and z-axes correspond to the width, length, and depth of the orifice respectively. For a fluid velocity of 10 μm s^{-1} in the channel-at-large, the maximum velocity in the orifice is 290 μm s^{-1}. (B) Experimentally measured (◆) and simulated (- - -) profile of normalized velocity of 9.9 μm diameter PS beads flowing through an 80 μm wide orifice.

Effect of orifice width on flow characteristics of microgels

Fig. 3 shows that both types of microgels experienced an increase in velocity as they approached and passed through the orifices, with the maximum velocity achieved near the center of the orifice. Unlike PS beads, microgel velocities did not increase as much as the continuous phase. Furthermore, microgels exhibited gradual velocity changes in the orifice (in contrast to the narrow velocity profiles in Fig. 2). We attribute these phenomena to the larger size, and larger drag force of the microgels, as well as to their compliance. In addition, as the microgels are water permeable, there is osmotic backflow through the microgel in the opposite direction of bulk flow.

We evaluated the variation in microgel velocity in five microchannels patterned with orifices with widths of 76, 80, 90, 125, and 200 μm. Fig. 3A shows that in the microchannels with orifices significantly wider than the particle diameter (*e.g.*, w = 125 μm), both types of microgels exhibited a similar increase in velocity of approximately 5.2-times the initial velocity of 250 μm s^{-1}. In contrast, in microchannels with narrow orifices relative to particle diameter (*e.g.*, w = 80 μm) (Fig. 3B), alginate microgels experienced a 9.8-fold increase in velocity whereas HTCC-alginate microgels experienced a 6.6-fold increase in velocity. We attribute this difference to electrostatic interactions between the particles and the walls of the orifice. Alginate microgels are negatively charged due to the presence of the carboxylate groups on the surface of the microgels. Thus, these particles are likely to be repelled by the negatively charged PDMS microchannel surface. In contrast, positively charged HTCC-alginate microgels are likely to experience an electrostatic attraction to the negatively charged

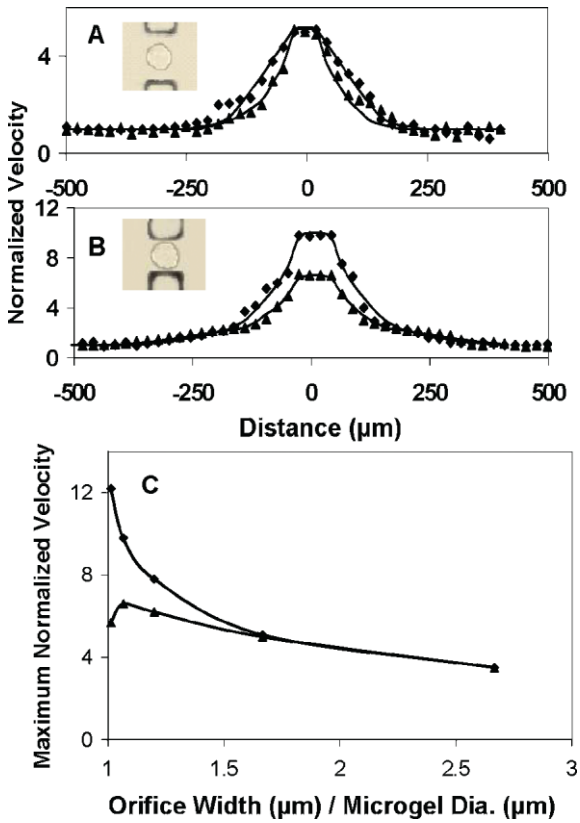

Fig. 3 Experimentally measured profile of normalized velocities of 75 μm-diameter alginate microgels (◆) and HTCC coated alginate microgels (▲), flowing through a 125 μm (A) and a 80 μm (B) wide orifice. (C) Comparison of orifice diameter. As the initial velocity increases (*i.e.*, time spent in the orifice decreases), the difference between the normalized velocities of the microgels decreases. Lines added for eye guidance only.

PDMS surface, which resulted in a smaller velocity increase in the orifice.

To further characterize the effect of orifice width on microgel flow, we evaluated the maximum normalized velocity of the microgels as a function of variation in the ratio of orifice width to microgel diameter. For orifices with $w > 90$ μm, we observed little or no effect on microgel flow. In contrast, in orifices with $w < 90$ μm (*i.e.*, the ratio of orifice width to microgel diameter below 1.2), the surface charge on microgel particles significantly affected their flow characteristics. We note that in the latter case the distances between microgel and orifice wall were from 0.5 to 7.5 μm, that is, significantly larger than what the range of distances expected for the interaction of two likely or oppositely charged surfaces.[42] Thus, we ascribe the observed effects to a slight misalignment of microgel motion with respect to the centre of the orifice (important for the flow of capsules through narrow orifices).

Effect of initial velocity of the dispersion in the microfluidic device on microgel flow characteristics

The effect of initial fluid velocity on the flow characteristics of microgels was evaluated in microchannels with orifice width $w = 80$ μm. As expected, the negatively charged alginate microgels experienced a larger increase in velocity than did HTCC-alginate microgels. In addition, a notable effect of initial velocity on microgel flow through the orifice was observed. For example, as shown in Fig. 4A, when solutions were driven at an initial velocity of 210 μm s^{-1}, alginate microgels experienced a two-fold larger increase in velocity than HTCC-alginate microgels. When propelled by a slower flow of 130 μm s^{-1}, the velocity increases for the two types of microgels differed by a factor of three (Fig. 4B).

The results of a systematic study of this effect are shown in Fig. 4C, where the maximum normalized velocity of the microgels is plotted as a function of the initial velocity of microgels. The maximum normalized velocity curves converge with increasing initial velocity, approaching unity at 800 μm s^{-1}. Thus, at high initial velocity, no difference was observed between the two types of microgels. These results stress two important effects. First, a compromise exists between the hydrodynamic forces generated by fluid flow and the interactions of microgels with orifice walls. Second, for low initial velocities, repulsive forces between the microchannel wall and the microgels have a more pronounced effect on microgel flow than attractive forces.

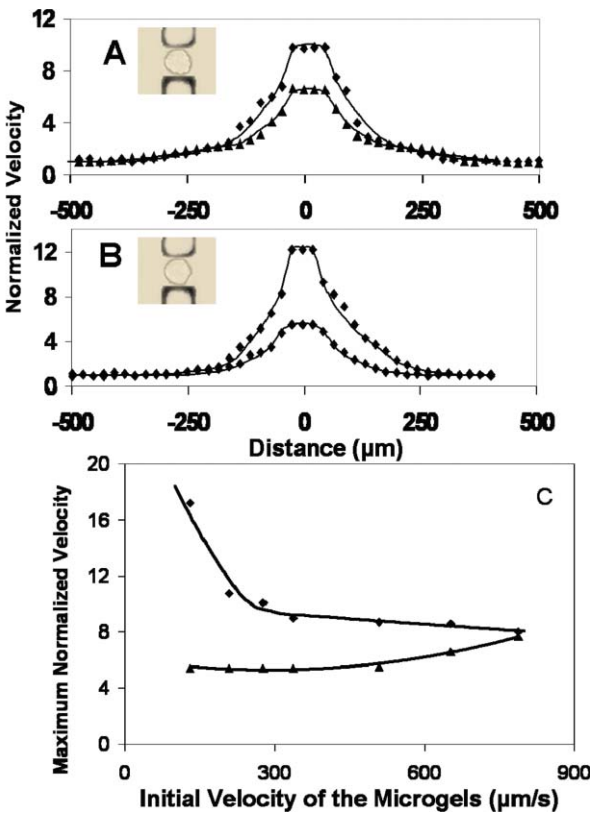

Fig. 4 Experimentally measured profile of normalized velocity of 75 μm diameter alginate microgels (◆) and HTCC coated alginate microgels (▲) flowing through an 80 μm wide orifice. The initial velocity of the microgels was 210 μm s^{-1} (A) and 130 μm s^{-1} (B). (C) Comparison of initial velocity of the microgels. As the initial velocity increase (*i.e.* time spent in the orifice decreases) the difference between maximum normalized velocities of the microgels. Lines added for eye guidance only.

Conclusions

We report the results of an experimental study of the flow characteristics of microgel capsules, by observing their velocities in orifices with varying dimensions. The electrostatic interaction between the microgels and the negatively charged microchannel surface was modulated by changing the surface functionality of the particles. Surface–surface interactions played a significant role in the flow dynamics of microgels when they passed through an orifice with dimensions comparable to the microgel diameters. Specifically, negatively charged 75 μm diameter microgels experienced an increase in velocity larger than that of positively charged microgels when flowing through orifices with widths <90 μm. These surface–surface interactions had greater effects when microgels were pushed at reduced flow rates through orifices, ranging from a three-fold difference between microgel types at 130 μm s^{-1} initial flow rate to virtually no difference at 800 μm s^{-1} initial flow rate. We expect that the described method will be generally useful for studies of the flow of suspensions of cells or other biologically relevant particles for a wide range of applications.

Acknowledgements

E. K and A. R. W thank NSERC and the CRC for the Canada Research Chair funding. The authors are grateful to Prof. Anna Balasz for fruitful discussions.

References

1 M. Das, H. Zhang and E. Kumacheva, *Annu. Rev. Mater. Res.*, 2006, **36**, 117–142.
2 R. G. Larson, *The Structure and Rheology of Complex Fluids*, Oxford University Press, New York, 1999.
3 M. Boissiere, P. J. Meadows, R. Brayner, C. Helary, J. Livage and T. Coradin, *J. Mater. Chem.*, 2006, **16**, 1178–1182.
4 M. T. Islam, N. Rodriguez-Hornedo, S. Ciotti and C. Ackermann, *Pharm. Res.*, 2004, **21**, 1192–1199.
5 J. de Vicente, J. R. Stokes and H. A. Spikes, *Food Hydrocolloids*, 2006, **20**, 483–491.
6 A. A. Khan, H. M. Khan and H. Delincee, *Food Control*, 2005, **16**, 141–146.
7 M. Villarini, G. Scassellati-Sforzolini, M. Moretti and R. Pasquini, *Cell Biol. Toxicol.*, 2000, **16**, 285–292.
8 V. C. Lopez, J. Hadgraft and M. J. Snowden, *Int. J. Pharm.*, 2005, **292**, 137–147.
9 O. Popanda, R. Ebbeler, D. Twardella, I. Helmbold, F. Gotzes, P. Schmezer, H. W. Thielmann, D. von Fournier, W. Haase, M. L. Sautter-Bihl, F. Wenz, H. Bartsch and J. Chang-Claude, *Int. J. Radiat. Oncol., Biol. Phys.*, 2003, **55**, 1216–1225.
10 D. J. Beebe, G. A. Mensing and G. M. Walker, *Annu. Rev. Biomed. Eng.*, 2002, 4.
11 D. J. Beebe, J. S. Moore, J. M. Bauer, Q. Yu, R. H. Liu, C. Devadoss and B.-H. Jo, *Nature*, 2000, 404.
12 G. Degre, P. Joseph, P. Tabeling, S. Lerouge, M. Cloitre and A. Ajdari, *Appl. Phys. Lett.*, 2006, 89.
13 S. Sato, D.-R. Chen and D. Y. H. Pui, *Aerosol Sci.*, 2002, 33.
14 M. E. Staben and R. H. Davis, *Int. J. Multiphase Flow*, 2004, 31.
15 X. Xuan and D. Li, *J. Micromech. Microeng.*, 2005, 16.
16 G. Fritz, W. Pechhold, N. Willenbacher and N. J. Wagner, *J. Rheol.*, 2003, **47**, 303–319.
17 K. A. Burridge, M. A. Figa and J. Y. Wong, *Langmuir*, 2004, **20**, 10252–10259.
18 E. Park, M. Smith, S. E. K. Snapp, J. DiVietro, W. Walker, D. Schmidtke, S. Diamond and M. Lawrence, *Biophys. J.*, 2002, **82**, 1835–1847.
19 S. Bhatia and D. Hammer, *Langmuir*, 2002, **18**, 5881–5885.
20 A. Eniola, P. Willcox and D. Hammer, *Biophys. J.*, 2003, **85**, 2720–2731.
21 Y. Zhang, V. Milam, D. Graves and D. Hammer, *Biophys. J.*, 2006, **90**, 4128–4136.
22 P. A. Stone, S. D. Hudson, P. Dalhaimer, D. E. Discher, E. J. Amis and K. B. Migler, *Macromolecules*, 2006, 39.
23 J. Beaucourt, F. Rioual, T. Seon, T. Biben and C. Misbah, *Phys. Rev. E*, 2004, 69.
24 R. H. Chen, H. P. Win and H. J. Fang, *J. Liposome Res.*, 2001, **11**, 211–228.
25 A. Fernandez-Nieves, A. Fernandez-Barbero and F. J. de las Nieves, *Phys. Rev. E*, 2001, 6304.
26 S. E. Paulin, B. J. Ackerson and M. S. Wolfe, *J. Colloid Interface Sci.*, 1996, **178**, 251–262.
27 A. Eniola and D. Hammer, *Biomaterials*, 2005, **26**, 7136–7144.
28 M. Fischlechner, L. Toellner, P. Messner, R. Grabherr and E. Donath, *Angew. Chem., Int. Ed.*, 2006, **45**, 784–789.
29 U. Reibetanz, C. Claus, E. Typlt, J. Hofmann and E. Donath, *Macromol. Biosci.*, 2006, **6**, 153–160.
30 S. Devasenathipathy, J. G. Santiago, S. T. Wereley, C. D. Meinhart and K. Takehara, *Exp. Fluids*, 2003, **34**, 504–514.
31 A. Alexeev, R. Verberg and A. C. Balazs, *Macromolecules*, 2005, **38**, 10244–10260.
32 A. Alexeev, R. Verberg and A. C. Balazs, *Soft Matter*, 2006, **2**, 499–509.
33 H. Moritaka, S. Kimura and H. Fukuba, *Food Hydrocolloids*, 2003, **17**, 653–660.
34 J. Wiedemair, M. J. Serpe, J. Kim, J. F. Masson, L. A. Lyon, B. Mizaikoff and C. Kranz, *Langmuir*, 2007, **23**, 130–137.
35 H. Zhang, E. Tumarkin, R. Peerani, Z. Nie, R. M. A. Sullan, G. C. Walker and E. Kumacheva, *J. Am. Chem. Soc.*, 2006, 128.
36 K. A. Burridge, M. A. Figa and J. Y. Wong, *Langmuir*, 2004, **20**, 10252–10259.
37 H. Zhang, S. Mardynano, W. C. Chan and E. Kumacheva, *Biomacromolecules*, 2006, 7.
38 P. Thibault, *Capillary Electrophoresis of Carbohydrates*, Humana Press, Totowa, NJ, 2003.
39 Y. N. Xia and G. M. Whitesides, *Angew. Chem., Int. Ed.*, 1998, 37.
40 A. L. London and R. K. Shah, *J. Eng. Power*, 1968, **90**, 218.
41 H. F. P. Purday, *An Introduction to the Mechanics of Viscous Flow (Streamline Flow)*, Dover Publications, Inc., New York, 1949.
42 J. N. Israelachvili, *Intermolecular and Surface Forces: With Applications to Colloidal and Biological Systems*, Academic Press, London, 1985.